

ANALYSIS OF FLOW STRUCTURE OF TUNNEL FIRE BASED ON MODAL DECOMPOSITION

by

Minggao CHEN, Jun MAO*, and Yanhong XI

School of Civil Engineering, Beijing Jiaotong University, Beijing, China

Original scientific paper

<https://doi.org/10.2298/TSCI211204107C>

In order to study the large scale flow structure of fire smoke in tunnels, this paper uses the excellent ability of proper orthogonal decomposition for the first time to extract flow field structure, processes the flow field data obtained from numerical simulation, obtains the 2-D and 3-D large-scale flow structure of fire smoke in tunnels and analyzes it. The proper orthogonal decomposition of temperature and velocity pulsation field shows that the proportion of first-order modal energy in temperature field is much higher than that in velocity field, indicating that the flow structure of velocity field is more complex than that of temperature field. Through modal phase analysis and modal decomposition of 3-D flow field, the influence of mode on fire smoke flow is recognized, and the understanding of tunnel fire smoke flow structure is deepened. The low-order mode is closely related to smoke flow. The increase of fire power has little effect on the reconstruction of flow field, and the cross-section energy recovery ratio near the fire source is higher under the same fire power.

Key words: *proper orthogonal decomposition, tunnel fire, modal decomposition, flow structure*

Introduction

According to statistics, when a tunnel fire broke out, the smoke spread caused great threats to the affected people, and about 85% of the casualties were caused by inhaling toxic smoke [1]. The temperature of fire smoke is higher than the ambient temperature and it flows longitudinally under the buoyancy drive. In the absence of longitudinal forced ventilation or when the intensity of longitudinal forced ventilation is small, the cold air downstream flows to the fire source to supplement the oxygen needed for combustion, and the fire smoke and the cold air move in opposite direction. The smoke flow in tunnel fire is closely related to turbulence. With the deepening of the understanding of turbulence, the initial random movement is transferred to the large-scale coherent structure, and the existence of large-scale coherent structure greatly affects the transport process. The large-scale structure of tunnel smoke is closely related to entrainment and heat transfer. It is very necessary to analyze and study the structure of smoke flow field for understanding the heat transfer and entrainment characteristics of fire smoke from the physical mechanism.

Modal decomposition technology is used to mathematically extract potential flow features from flow field data or flow evolution operators. We refer to modal decomposition as a mathematical technique to extract important characteristics of fluids in terms of energy and

* Corresponding author, e-mail: jmao@bjtu.edu.cn

dynamics. The spatial characteristics of flows are called (spatial) modes. The input object of modal decomposition is flow field data, which can be either numerical simulation data or experimental data. Therefore, modal decomposition is also a data-based technology [2]. Proper orthogonal decomposition (POD) is a widely used modal decomposition method. The POD is also known as Karhunen-Loe've Decomposition, Principal Component Analysis, Singular Value Decomposition, Empirical Eigenfunction Decomposition, *etc.* The method was independently discovered by different scientists [3]. In this method, the flow field is divided into the combination of space and time from the massive and high dimensional data, and the non-linear system is treated with linear order reduction according to the energy contribution rate of each order mode, and the large-scale coherent structure is obtained by using the low order mode. Lumley [4] was the first to introduce it into the field of fluid dynamics turbulence and extract coherent structures from turbulent flow fields. With the increase of data volume, Sirovich [5] proposed the snapshot POD method. Applications of POD technology mainly include basic analysis of fluid flow [6-8], order reduction modelling [9, 10], data compression/reconstruction [11], flow control and aerodynamic design [12, 13], *etc.*

The research on the smoke movement of tunnel fire mainly focuses on the maximum temperature rise under the roof [14-16], smoke transport [17-20], critical wind speed [21-23], longitudinal attenuation law of temperature [24, 25], and shaft smoke exhaust [26, 27], fire risk assessment [28]. The research methods include full-scale experiment, model experiment and numerical simulation. Although many laws and conclusions have been obtained from the aforementioned studies, there are few studies on the large-scale flow structure in flue gas and the relationship between the structure and heat transfer and entrapment. The POD has successfully extracted large-scale flow structures in the field of fluid mechanics [29], but its application in fire smoke is rare. Yang *et al.* [30] extracted the large-scale flow structure of fire-induced buoyancy plume by using POD. Therefore, this paper combined with POD method, made use of its excellent ability to extract flow field structure, processed the flow field data obtained from numerical simulation, and obtained the large-scale flow structure of tunnel fire smoke and analyzed it.

Used methods

The proper orthogonal decomposition

The study object of the POD method can be either a scalar field (temperature) or a vector field (velocity). For the instantaneous flow field at a moment i , sampling is carried out at m spatial positions and arranged into a column vector in a certain order, which can be called a snapshot of the flow field. The snapshot of the flow field at N moments constitutes matrix A containing the spatial and temporal information in the original flow field:

$$A = \begin{pmatrix} a_{11} & \cdots & a_{1N} \\ \vdots & \ddots & \vdots \\ a_{m1} & \cdots & a_{mN} \end{pmatrix} \quad (1)$$

The POD method decomposes the pulsation in the original flow field into a combination of space and time, that is, the combination of the modal basis function and the time coefficient:

$$q(\varepsilon, t) - \bar{q}(\varepsilon) = A = \sum_j a_j(t) \varphi_j(\varepsilon) \quad (2)$$

where $\bar{q}(\varepsilon)$ is the average value of flow field, $a_j(t)$ – the time coefficient, $\varphi_j(\varepsilon)$ – the modal basis function, and $a_j(t)\varphi_j(\varepsilon)$ – the modal.

The $C = A^T A$ is the time correlation matrix, λ_j , α_j are eigenvalues and eigenvectors of matrix C:

$$\varphi_j(\varepsilon) = \frac{1}{\sqrt{\lambda_j}} A \alpha_j(t) \quad (3)$$

$$a_j(t) = [\varphi_j(\varepsilon)]^T A \quad (4)$$

Simulation model

The fire dynamics simulator (FDS) is a CFD tool designed specifically for low-speed and thermally driven flow rate large-scale eddy current simulation (LES) and has been widely used in fire research and its effectiveness has been widely proven. The model tunnel in numerical simulation was constructed according to the experimental model in the literature of Lee and Ryou [31]. The experimental model was a 1/20 scale ratio model with a length of 10.4 m and a width to height ratio of 1:1 and 0.4 m, fig. 1. In this paper, FDS was used to establish a numerical model of the same size scale. A total of seven temperature monitoring points were set at the longitudinal interval of every meter on the top of the tunnel, and 18 temperature monitoring points were set along the vertical direction 2 m away from the fire source.

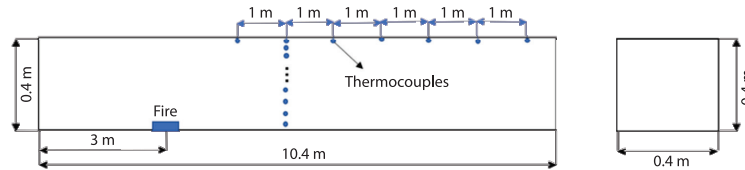


Figure 1. Tunnel model and lay-out of measuring points

Mesh sensitivity analysis

In order to ensure the accuracy of the numerical simulation, the grid independence and the accuracy of the numerical simulation must be verified first. The FDS user manual recommends using D^*/δ_x to evaluate mesh size [32]. The fire characteristic diameter, D^* , is expressed:

$$D^* = \left(\frac{Q}{\rho_0 c_p T_0 g^{1/2}} \right)^{2/5} \quad (5)$$

The D^*/δ_x is recommended for 4-16. Taking an 8 kW HRR as an example, the recommended mesh size range is 0.0084-0.035 m. Therefore, 0.014 m, 0.016 m, 0.02 m, 0.025 m and 0.03 m were selected as grid sizes within the recommended range for grid independence verification.

The fig. 2 shows the vertical temperature distribution at two meters away from the fire source with different mesh sizes. As can be seen from the figure, with the decrease of the grid size, the temperature distribution in the vertical direction tends to be uniform. It is found that when the grid size is

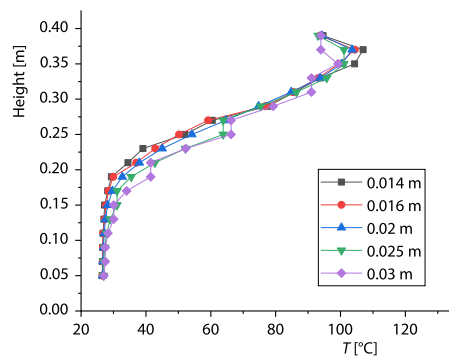


Figure 2. Grid independence verification

0.016 m, the temperature changes little compared with 0.014 m. That is, when the grid size is less than 0.016 m, the calculation result does not significantly improve and the calculation time increases. Therefore, the grid size is chosen as 0.016 m.

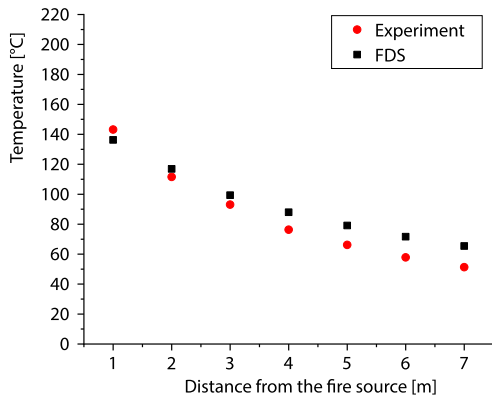


Figure 3. Comparison between numerical simulation and scale experiment data

Model validation

Lee and Ryou [31] experiment monitored the longitudinal temperature distribution of an 8.27 kW fire source. Set a thermocouple at the top of the tunnel at intervals of 1 m from the fire source. The FDS was used to simulate the experiment, the grid size is chosen as 0.016 m and the experimental data and numerical simulation results were compared

It can be seen from the fig. 3 that the simulation results of longitudinal temperature are in good agreement with the experimental data, so it can be considered that FDS is accurate for numerical simulation of fire.

Modal decomposition region selection

The spread of smoke can be divided into four stages:

- plume rising stage,
- radial spreading stage,
- transition stage, and
- the 1-D spreading stage.

The 4.2 m cross-section corresponds to the transition stage, the 7 m cross-section corresponds to the 1-D propagation stage, and the 10 m cross-section corresponds to the inflow of a large amount of cold air at the tunnel outlet. Longitudinal sections are taken from the center of the fire source, and the cross-sections are taken from the longitudinal 4.2 m, 7 m, and 10 m of the tunnel to be used as the region of 2-D POD. Physical quantities at different moments in the region are extracted as the objects of decomposition.

The area from 4.2 m to 5 m is a transitional stage, therefore, it is regarded as a 3-D decomposition area. In the process of 3-D decomposition, the cross-sections of 4.2 m, 4.4 m, 4.6 m, 4.8 m, and 5 m were taken as the decomposition area, fig. 4, and the velocity and temperature at different moments in the area were extracted as the decomposition objects.

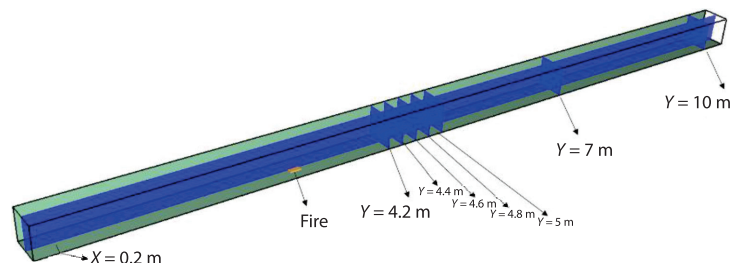


Figure 4. The POD cross-sectional schematic

Results and discussion

Verification of modal convergence

The modal decomposition data were calculated by FDS software. Using MATLAB software to write a program to realize the pod algorithm, and decompose the flow field data obtained by numerical simulation. Mixing and entrainment of fire smoke are closely related to the flow structure. The method of POD can effectively separate the flow structure. Firstly, the convergence verification of flow snapshot should be carried out. Referring to the article of Huang *et al.* [33], When the energy ratio of each mode varies little under different flow field snapshots, the number of flow field snapshots is considered to converge.

As can be seen from the fig. 5, as the number of snapshots in the flow field increases, the energy proportion of each order mode changes. When the number of snapshots is 500, if the number of snapshots is increased, the energy proportion of each order mode no longer changes, so it can be considered that the number of snapshots in the flow field converges at this time.

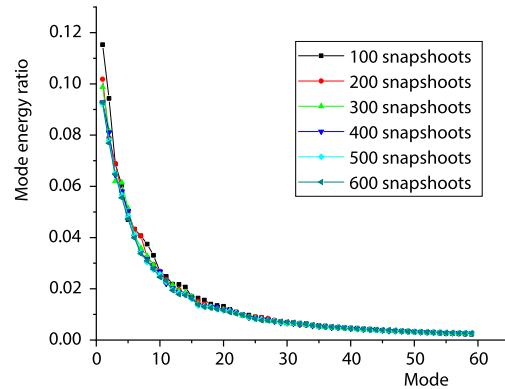


Figure 5. Energy ratio of each mode under different number of flow field snapshots

Modal analysis of velocity field and temperature field

Through the analysis of temperature and velocity fluctuation, the disturbance in the flow field is mainly caused by the interaction between the smoke and the tunnel wall and the inflow of fresh air. In order to further study the dominant temperature mode and turbulence coherent structure in the flow field, the temperature and velocity pulsation fields were decomposed by POD, and the energy proportion of each order mode and the first four order modes at different sections were obtained as shown in the figs. 6 and 7. The energy ratio of the 25th order mode is only about 1%, and the energy of the subsequent high-order modes is lower. Therefore, only the energy proportion curve of the first 25 modes is given in this paper.

As can be seen from the fig. 6, the energy of the lower order mode is larger. With the increase of the order number, the energy proportion of each order mode decreases gradually,

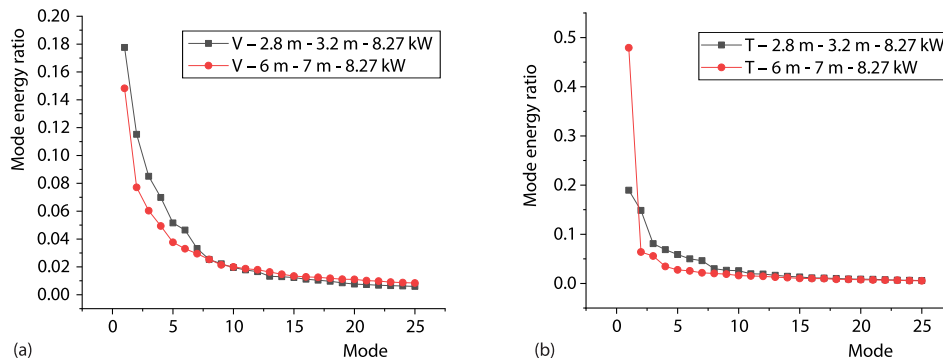


Figure 6. The energy ratio of each mode of (a) velocity pulsation field and (b) temperature pulsation field at different longitudinal positions of the tunnel

indicating that the low-order mode represents the large-scale flow structure in the flow field, while the high-order mode represents the small-scale flow structure. Due to shear entrainment and energy transfer in the flow field, the large-scale vortex structure with high energy breaks down into small scale structure with low energy, and finally dissipates.

By decomposing the velocity field and temperature field at the fire source, it can be seen from the fig. 7 that the first and second modes of the velocity field represent the large-scale vortex structure in the plume rising stage. Mode 3 and 4 represent the impact of the plume structure on the tunnel roof. Because of the existence of these large-scale vortex structures, the flue gas absorbs a lot of fresh air and the mass-flow rate of flue gas increases rapidly.

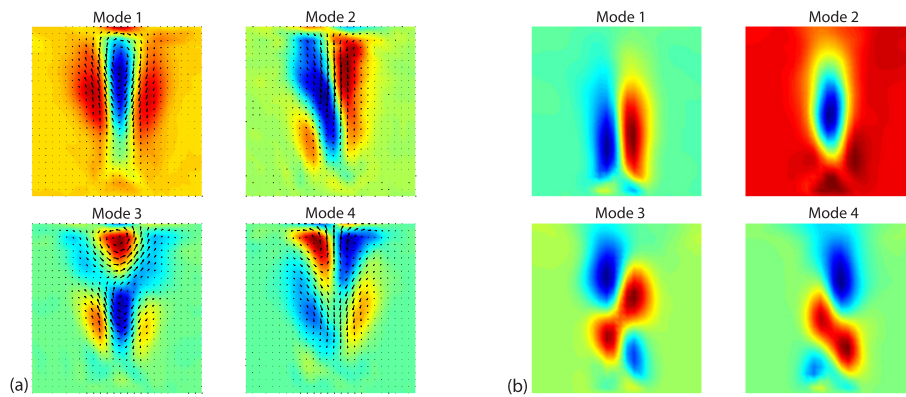


Figure 7. The four modes of (a) velocity field and (b) temperature field at the longitudinal 2.8-3.2 m fire source of the tunnel

For the cross-sections at different positions, fig. 8, compared with the energy proportion of each order of the velocity field, the energy of each order of the temperature field accounts for a larger proportion. At the cross-section of 7 m, the first-order mode energy accounts for 55%, and the maximum value of the first-order mode energy obtained by velocity field decomposition is 6%, indicating that the structure of velocity field at the cross-section is more complex than that of temperature field.

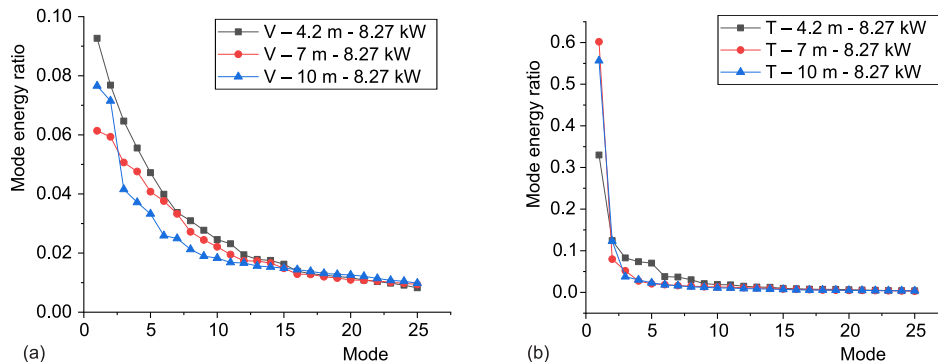


Figure 8. The energy ratio of each mode of velocity pulsation field and temperature pulsation field in 4.2 m, 7 m, and 10 m cross-section; (a) and (b)

The fig. 9 represents the spatial distribution diagram of velocity vector and vorticity of the first four modes of velocity pulsation field obtained by POD decomposition. It can be seen from the figure that due to the difference of flue gas movement, the modes of the same

order at different sections have significant differences. For the 4.2 m cross-section near the fire source and the 7 m cross-section in the middle of the tunnel, the smoke movement of these two cross-sections is mainly concentrated in the upper part of the tunnel and the tunnel wall, and the spatial distribution of each order mode is mainly concentrated in the upper part. Due to the supplementary inflow of fresh air, the modal spatial distribution at the 10 m cross-section is mainly concentrated in the lower part. The first mode of the 4.2 m cross-section is a vortex that rotates clockwise in the central region of the upper section. As the mode coefficient will change with time, this mode represents the alternating shedding of the vortex in the middle of the tunnel. The second-order mode is two vortices rotating in opposite directions at the upper part of the tunnel, which represents the vortices falling off alternately in opposite directions under the influence of tunnel wall. The second-order and fourth order modes of the 10 m cross-section are similar to the first-order and second-order modes of the 4.2 m cross-section, except that the position of the vortex is lower and is caused by the inflow of fresh air.

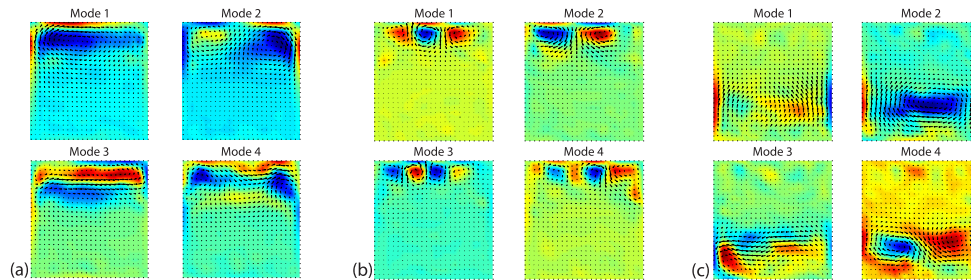


Figure 9. The four modes of velocity pulsation field decomposition in 4.2 m (a), 7 m (b), and 10 m (c) cross-sections

The fig. 10 represents the spatial distribution diagram of the first four modes of temperature pulsation field obtained by POD decomposition. Combined with the energy proportion diagram, it can be known that the first mode is the dominant mode. The first mode represents the vertical temperature change and represents the temperature stratification. The energy of mode 2-4 of the 4.2 m cross-section is higher than that of other sections, and there are alternately positive and negative pulsation regions, which represent the change of temperature along the transverse direction. These regions are distributed in the upper part of the tunnel. From the modal diagrams of the temperature pulsation field of three cross-sections, it can be seen that the area with drastic changes coincides with the area of the velocity pulsation vorticity of the hot flue gas, indicating that the temperature pulsation mode is closely related to the flue gas movement. It shows that the temperature changes dramatically due to the eddy motion of the flue gas.

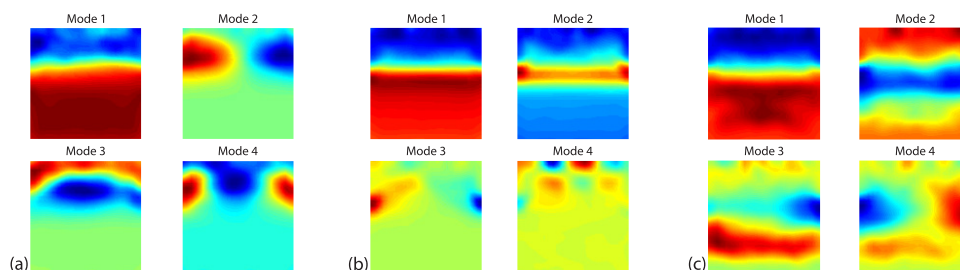


Figure 10. The four modes of temperature pulsation field decomposition in 4.2 m (a), 7 m (b), and 10 m (c) cross-sections

Phase analysis

The time coefficient A_j of each mode represents the change rule of the mode with time. Taking the section of 7 m as an example, the time coefficients of the first four modes obtained by velocity field decomposition are shown in the fig. 11.

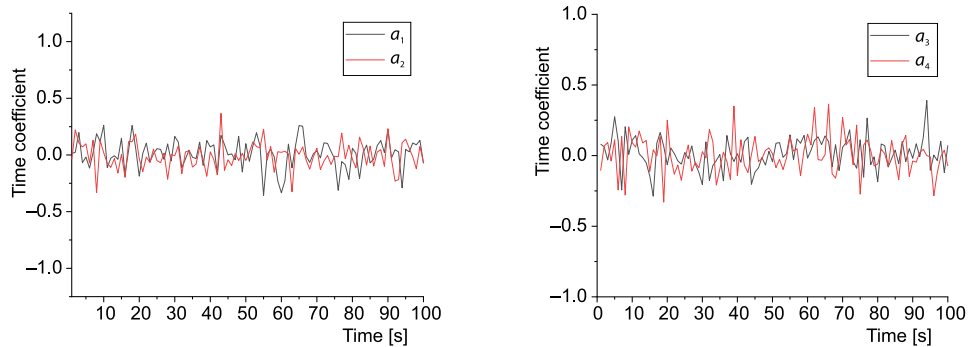


Figure 11. The time coefficient of the first four modes of the velocity pulsation field in the 4.2 m section varies with time

As can be seen from the fig. 11, the time coefficients of each mode fluctuate around the value of 0 with the growth of time, and have a certain periodicity. Power spectral density analysis was performed on the modal time coefficient, as shown in the fig. 12.

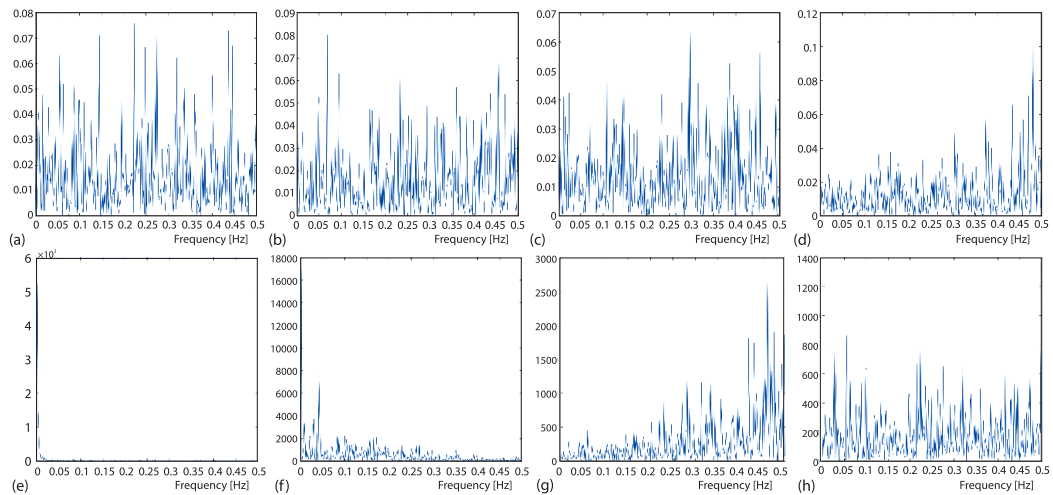


Figure 12. Power spectral density analysis of four modes time coefficients of velocity field (a)-(d), and temperature field (e)-(h) in 7 m cross-section

As can be seen from the fig. 12, the modes identified by POD have multiple frequencies, and the flow structure with a single frequency cannot be separated by this method. Compared with the frequency identified by temperature field, the modal frequency of velocity field is generally higher than that of temperature field, because the movement of flue gas is faster than the speed of heat transfer.

In order to better understand the flow structure corresponding to each mode and reproduce the generation of vortices in the instantaneous flow field, we can use the time coefficients of the first two modes to determine the phase information related to vortices [34]. The a_1 and

a_2 are not independent of each other, while statistically unrelated. Firstly, the time coefficients of the first two modes are normalized dimensionally:

$$a_i^* = \frac{a_i}{\sqrt{2\lambda_i}}, \quad i = 1, 2 \quad (6)$$

The fig. 13 shows the correlation of the normalized time coefficients of the first two modes. All points can be grouped into a circle of radius 3. Phase angle, θ , can be considered a_1^* and a_2^* angle in the plane. The phase angle θ is defined:

$$\theta(t) = \arctan \left[\frac{a_2^*(t)}{a_1^*(t)} \right] \in [-\pi, \pi] \quad (7)$$

The relationship between a_1^* and a_2^* and phase angle θ is shown in the fig. 14.

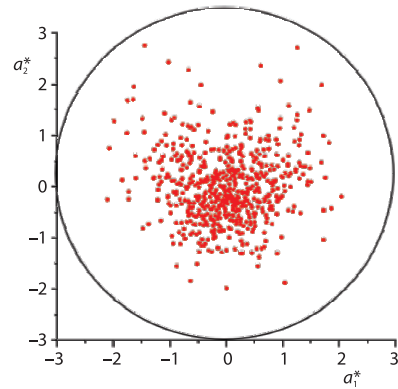


Figure 13. Normalized scatter plot of modal time coefficient

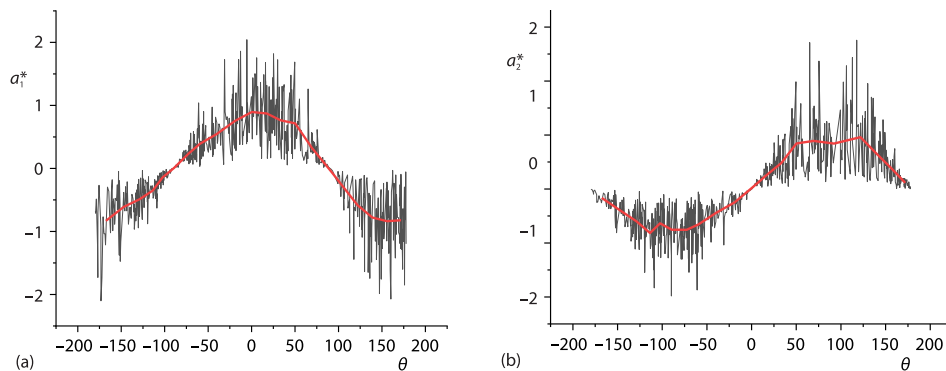


Figure 14. The relationship between (a) a_1^* and (b) a_2^* and phase angle θ

As can be seen from the fig. 14, the values of a_1^* and a_2^* fluctuate greatly, so they are averaged, and the curve between the averaged values and the phase angle θ is shown in the figure. The values of a_1^* and a_2^* can be assigned within the range $[-\pi, \pi]$. The changes of the reconstructed flow field after the superposition of the first-order mode and the second-order mode at different phases are shown in the fig. 15.

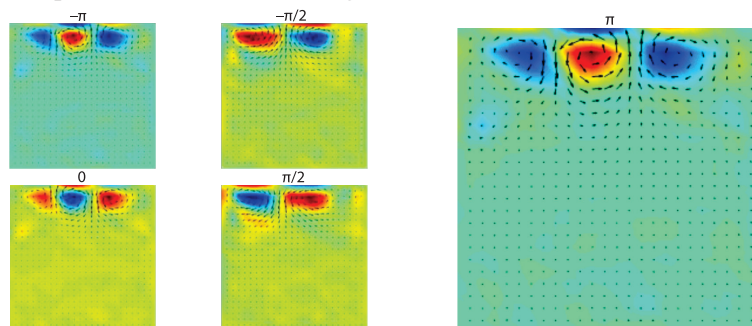


Figure 15. Representation of the flow field in different phases after the reconstruction of the first two modes

Changes of the reconstructed flow field after superposition of the average flow field, first-order mode and second-order mode under different phases are shown in the fig. 16.

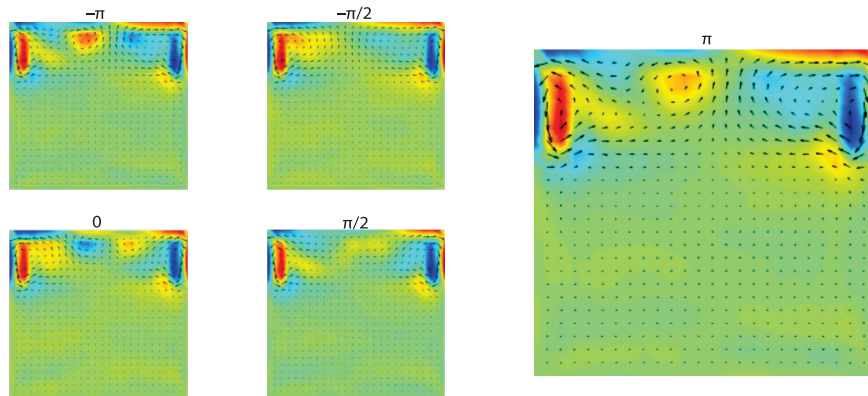


Figure 16. Representation of the flow field in different phases after the reconstruction of the first two modes and the mean flow field

The average flow field is steady flow, and the first and second order modes are unsteady flow. It can be seen from the figure that the flow field change after superposition is a periodic process. When the phase is $-\pi$, the flow field after the superposition of the first two modes is centered by a counterclockwise rotating vortex with clockwise rotating vortices on both sides. The average flow field is two opposite vortices near the tunnel wall. After superposition of the aforementioned flow field and the average flow field, it is found that after superposition of the first two modes, the clockwise swirling vortex on the left side of the tunnel wall is offset by the counterclockwise swirling vortex on the left side of the tunnel wall. As a whole, there are two vortices in opposite directions at the upper part of the tunnel, which are in the same direction as the swirling vortex on the tunnel wall. When the phase is $-\pi/2$, the vortex after superposition of the first two modes has the same rotation direction as the tunnel wall vortex, and both of them enhance the motion of the tunnel wall vortex. When the phase is 0, the vortex after the superposition of the first two modes changes. After superposition with the average flow field, the left counterclockwise rotating vortex enhances the motion of the left tunnel wall vortex. The vortex in the upper part of the tunnel is in the opposite direction the vortex in the upper part of the tunnel when the phase is $-\pi$. When the phase is $\pi/2$, the vortex after superposition of the first two modes has the opposite rotation direction the tunnel wall vortex, which weakens the motion of the tunnel wall vortex. When the phase is π , the motion of the vortex is consistent with the phase of $-\pi$, completing a periodic cycle. It can be seen that the superposition of the first two modes has different effects on the vortex motion of the tunnel wall under different phases. The first two modes represent only two kinds of flow field structures with high energy. Because the flow field is too complex, the movement of the complete flow field cannot be completely reproduced by the superposition of the first two modes alone. However, this method can make us better understand the movement of large-scale structure in the flow field and enrich the research content of tunnel fire smoke.

The 3-D flow field decomposition

The flow field data of the regions between the tunnels 4.2-5 m is extracted. The average flow field and the first two-order modality obtained after 3-D POD of the flow field and the first two-order modality as shown in fig. 17.

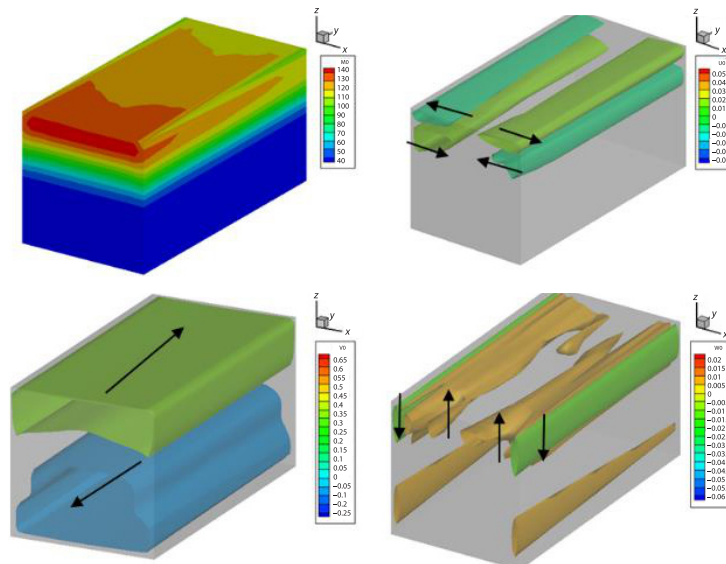


Figure 17. The 3-D decomposition average flow field of temperature field and velocity field

The longitudinal direction of the 3-D temperature field is longitudinally reduced, and the vertical direction has a significant temperature stratification. The speed equation of the horizontal speed, U , and the vertical velocity, W , is the positive and negative alternate, the upper right of the horizontal speed, U , is positive, the lower right is negative, the vertical speed, W , is positive, close to the upper right corner, close to the tunnel wall is negative, Looking in the y -axis, it is a vortex to rotate counterclockwise. Similarly, the upper left corner is a scroll rotating clockwise, corresponding to the 2-D average field. The average field velocity equivalent surface of the longitudinal velocity, V , is negative, characterized by the longitudinal movement of the thermos of the tunnel, and the cold air-flows from the lower portion along the tunnel.

As can be seen from the fig. 18, the lower right corner of the first-order mode of velocity, U , is negative and positive, which represents the flow to the left and right, and the lower right corner of the first-order mode of velocity, W , is negative and positive, which represents the flow to the down and up. From the Y -axis direction, it represents the clockwise rotating vortex. The first-order mode of velocity, V , is positive and negative alternately, which indicates that the flue gas-flows longitudinally along the tunnel and the cold air-flows into the tunnel. The second-order modes of velocity, W , and velocity, W , represent the clockwise rotating vortex in the upper part of the tunnel. It can be seen that the motion of modal representation obtained by 3-D decomposition is different from that obtained by 2-D decomposition.

The HRR and modal relationship

This paper also analyzes the modes under different fire source power. The fire source is divided into three, 8.27 kW, 12.5 kW, and 16 kW. The energy proportion of each mode obtained by pod decomposition of velocity field and the energy recovery ratio obtained by superposition of previous modes are sorted out.

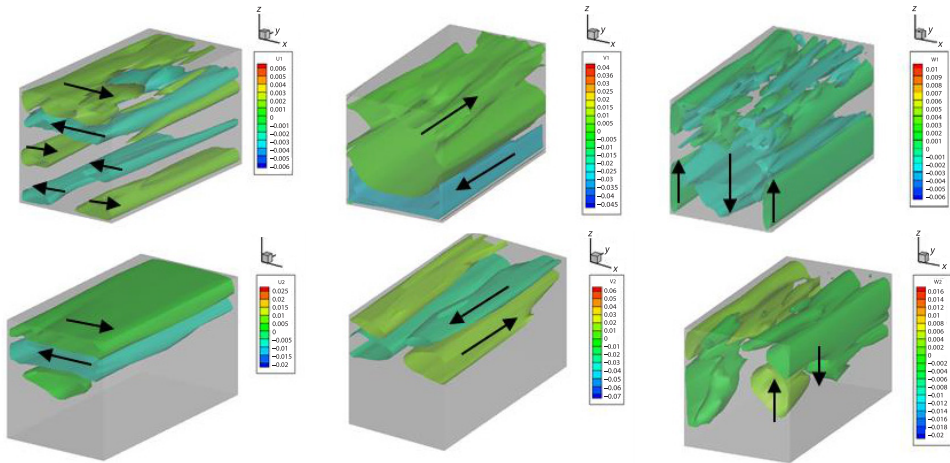


Figure 18. The first two POD modes obtained from the decomposition of velocity components U , V , and W

It can be seen from the fig. 19 that for the section near the fire source, the first few modal energy obtained by modal decomposition accounts for a relatively high proportion, and the modal energy obtained by section decomposition in the middle of the tunnel accounts for a relatively low proportion. When the power of fire source increases, the change of energy proportion in the same cross-section is small.

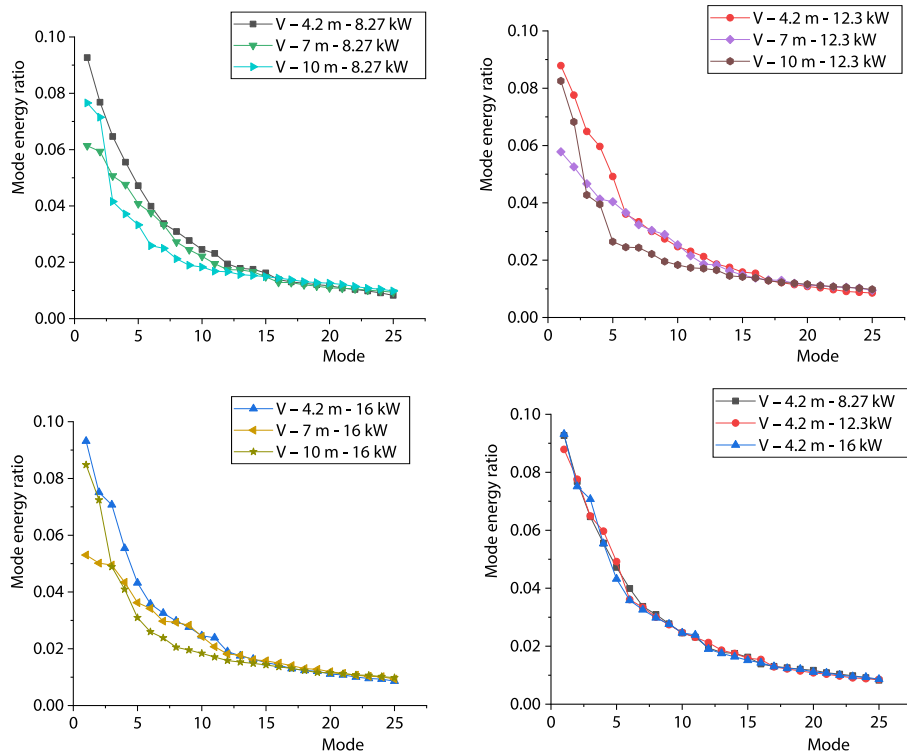


Figure 19. Energy ratio of the first 25 modes of three sections

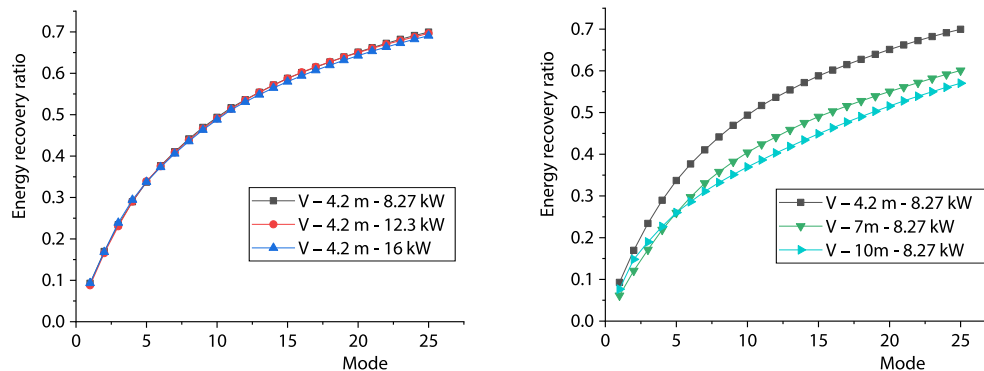


Figure 20. The reconstruction energy recovery ratio of the same cross-section with different power and different cross-section with the same power flow field

The top 25-order superimposed energy recovery ratio of different fire sources at the same cross-section can reach 0.7, and the increase in fire source power is less impact on the reconstruction of the flow field. The energy recovery ratio of modal superposition at different cross-sections of the same fire source power can be seen in the fig. 20 that the energy recovery ratio of cross-section near the fire source is high.

Conclusion

This paper analyzes the flow field of tunnel fire flue gas, found that the cause of flowing fluctuations is the flow of thermos and the flow of fresh air in the tail of the tunnel. The POD method is introduced to decompose the flow field in time and space, and extract the characteristic structure of the flow field. The results show that this method can effectively extract the large-scale coherent structure of temperature fluctuation field and velocity fluctuation field. The structure of velocity fluctuation field is more complex than that of temperature fluctuation field, and the flow field structure obtained by decomposition of temperature fluctuation field is closely related to the flow structure obtained by decomposition of velocity fluctuation field. The time coefficient obtained by POD decomposition contains flow structures with multiple frequencies. The large-scale flow structure decomposed by POD method is helpful to deepen the understanding of tunnel fire flow field. The decomposed low-order modes are closely related to flue gas-flow. The increase of fire power has little effect on the reconstruction of flow field. The energy recovery ratio of the cross-section near the fire source is higher for the same fire source power.

Acknowledgment

Natural Science Foundation of China (Grant No. 52172336;51578061; 52072027), the Fundamental Research Funds for the Central Universities (Grant No. 2019JBM087), Shenzhen construction engineering scientific research project (Grant No. BYTD-KT-002).

References

- [1] Alarie, Y., Toxicity of Fire Smoke, *Critical Reviews in Toxicology*, 32 (2002), 4, pp. 259-289
- [2] Taira, K., et al., Modal Analysis of Fluid-Flows: An Overview, *Aiaa Journal*, 55 (2017), 12, pp. 4013-4041
- [3] Berkooz, G., et al., The Proper Orthogonal Decomposition in the Analysis of Turbulent Flows, *Annual Review of Fluid Mechanics*, 25 (1993), 1, pp. 539-575
- [4] Lumley, J. L., The Structure of Inhomogeneous Turbulent Flows, in: *Atmospheric Turbulence and Radio Wave Propagation*, (Eds. Yaglom, A. M., Tartarsky, V. I.), Defence Tech. Info. Centre, Fort Belvoir, Va., USA, 1967, pp. 166-177

- [5] Sirovich, L., Turbulence and the Dynamics of Coherent Structures, I. Coherent Structures, *Quarterly of Applied Mathematics*, 45 (1987), 3, pp. 561-571
- [6] Murray, N., et al., Properties of Subsonic open Cavity Flow Fields, *Physics of Fluids*, 21 (2009), 9, pp. 479-178
- [7] Liu, Z. C., et al., Reynolds Number Similarity of Orthogonal Decomposition of the Outer Layer of Turbulent Wall Flow, *Physics of Fluids*, 6 (1994), 8, pp. 2815-2819
- [8] Cazemier, W., et al., Proper Orthogonal Decomposition and Low-Dimensional Models for Driven Cavity Flows, *Physics of Fluids*, 10 (1998), 7, pp. 1685-1699
- [9] Aubry, N., et al., The Dynamics of Coherent Structures in the Wall Region of a Turbulent Boundary-Layer, *Journal of Fluid Mechanics*, 192 (1988), July, pp. 115-173
- [10] Noack, B. R., et al., *Reduced-Order Modelling for Flow Control*, Springer Science and Business Media, New York, USA, 2011
- [11] Willcox, K., Unsteady Flow Sensing and Estimation Via the Gappy Proper Orthogonal Decomposition, *Computers and fluids*, 35 (2006), 2, pp. 208-226
- [12] Bui-Thanh, T., et al., Aerodynamic Data Reconstruction and Inverse Design Using Proper Orthogonal Decomposition, *AIAA Journal*, 42 (2004), 8, pp. 1505-1516
- [13] Edstrand, A. M., et al., Active Attenuation of a Trailing Vortex Inspired by a Parabolized Stability Analysis, *Journal of Fluid Mechanics*, 855 (2018), Nov., R2
- [14] Alpert, R. L., Calculation of Response Time of Ceiling-Mounted Fire Detectors, *Fire Technology*, 8 (1972), 3, pp. 181-195
- [15] Kurioka, H., et al., Fire Properties in Near Field of Square Fire Source with Longitudinal Ventilation in Tunnels, *Fire Safety Journal*, 38 (2003), 4, pp. 319-340
- [16] Hu, L., et al., On the Maximum Smoke Temperature under the Ceiling in Tunnel Fires, *Tunnelling and Underground Space Technology*, 21 (2006), 6, pp. 650-655
- [17] Ji, J., et al., Effects of Ambient Pressure on Transport Characteristics of Thermal-Driven Smoke Flow in a Tunnel, *International Journal of Thermal Sciences*, 125 (2018), Mar., pp. 210-217
- [18] Wu, J., Shen, F., Experimental Study on the Effects of Ventilation on Smoke Movement in Tunnel Fires, *International Journal of Ventilation*, 15 (2016), 1, pp. 94-103
- [19] Ji, J., et al., Experimental Investigation on Influence of Different Transverse Fire Locations on Maximum Smoke Temperature under the Tunnel Ceiling, *International Journal of Heat and Mass Transfer*, 55 (2012), 17-18, pp. 4817-4826
- [20] Jiang, X., et al., Study on Air Entrainment Coefficient of 1-D Horizontal Movement Stage of Tunnel Fire Smoke in Top Central Exhaust, *Tunnelling and Underground Space Technology*, 60 (2016), Nov., pp. 1-9
- [21] Atkinson, G., Smoke Movement Driven by a Fire under a Ceiling, *Fire Safety Journal*, 25 (1995), 3, pp. 261-275
- [22] Wu, Y., Bakar, M. A., Control of Smoke Flow in Tunnel Fires Using Longitudinal Ventilation Systems – A Study of the Critical Velocity, *Fire Safety Journal*, 35 (2000), 4, pp. 363-390
- [23] Li, Y. Z., et al., Study of Critical Velocity and Backlayering Length in Longitudinally Ventilated Tunnel Fires, *Fire Safety Journal*, 45 (2010), 6-8, pp. 361-370
- [24] Ingason, H., Li, Y. Z., Model Scale Tunnel Fire Tests with Longitudinal Ventilation, *Fire Safety Journal*, 45 (2010), 6-8, pp. 371-384
- [25] Liu, C., et al., Temperature Profile of Fire-Induced Smoke in Node Area of a Full-Scale Mine Shaft Tunnel under Natural Ventilation, *Applied Thermal Engineering*, 110 (2017), Jan., pp. 382-389
- [26] Yoon, C. H., et al., The Evaluation of Natural Ventilation Pressure in Korean Long Road Tunnels with Vertical Shafts, *Tunnelling and Underground Space Technology*, 21 (2006), 3, pp. 472-472
- [27] Yuan-Dong, H., et al., Effects of the Ventilation Duct Arrangement and Duct Geometry on Ventilation Performance in a Subway Tunnel, *Tunnelling and Underground Space Technology incorporating Trenchless Technology Research*, 26 (2011), 6, pp. 725-733
- [28] Vidmar, P., Risk Evaluation in Road Tunnels Based on CFD Results, *Thermal Science*, 26 (2022), 2, pp. 1435-1450
- [29] Chao, X., et al., Unsteady Flow Structures in the Wake of a High-Speed Train, *Experimental Thermal & Fluid Science*, 98 (2018), Nov., pp. 381-396
- [30] Yang, D., et al., The Application of Snapshot POD Method in Characterization and Analysis of Numerically Simulated Fire-Induced Flows, *Proceedings, Heat Transfer Summer Conference*, San Francisco, Cal., USA, 2009, Vol. 3, pp. 41-61
- [31] Lee, S. R., Ryou, H. S., An Experimental Study of the Effect of the Aspect Ratio on the Critical Velocity in Longitudinal Ventilation Tunnel Fires, *Journal of Fire Sciences*, 23 (2005), 2, pp. 119-138

- [32] McGrattan, K., *et al.*, Fire Dynamics Simulator User's Guide, NIST Special Publication, 1019 (2013), 6, pp. 1-339
- [33] Huang, T., *et al.*, Flow Dynamics and Heat Transfer Characteristics Analysis for Flootation Nozzle Using Large Eddy Simulation and Proper Orthogonal Decomposition Method, *International Journal of Thermal Sciences*, 155 (2020), 106402
- [34] Van Oudheusden, B., *et al.*, Phase-Resolved Characterization of Vortex Shedding in the Near Wake of a Square-Section Cylinder at Incidence, *Experiments in Fluids*, 39 (2005), 1, pp. 86-98